Journal of Alloys and Compounds 721 (2017) 586–592

Contents lists available at ScienceDirect

Journal of Alloys and Compounds

journal homepage: http://www.elsevier.com/locate/jalcom

The effect of fission-energy Xe ion irradiation on dissolution of UO_2 thin films

Aleksej J. Popel [a, *], Vladimir G. Petrov [b], Vasily A. Lebedev [b, c], Jason Day [a], Stepan N. Kalmykov [b, d], Ross Springell [e], Thomas B. Scott [e], Ian Farnan [a]

[a] Department of Earth Sciences, University of Cambridge, Downing Street, Cambridge, CB2 3EQ, United Kingdom
[b] Department of Chemistry, Lomonosov Moscow State University, Moscow, 119991, Russia
[c] Department of Materials Science, Lomonosov Moscow State University, Moscow, 119991, Russia
[d] National Research Centre "Kurchatov Institute", 123098, Moscow, Russia
[e] Interface Analysis Centre, School of Physics, University of Bristol, Bristol, BS8 1TL, United Kingdom

ARTICLE INFO

Article history:
Received 23 January 2017
Received in revised form
18 April 2017
Accepted 7 May 2017
Available online 10 May 2017

Keywords:
UO_2
Ion irradiation
Radiation damage
Ion-beam-induced mixing
Dissolution
Secondary phases

ABSTRACT

The aim of this work was to study the effect of fission fragment damage on the dissolution of UO_2 thin films in water. For this purpose, thin films of UO_2 on LSAT ($Al_{10}La_3O_{51}Sr_{14}Ta_7$) substrates were produced and irradiated by 92 MeV $^{129}Xe^{23+}$ ions to a fluence of 4.8×10^{15} ions/cm^2 to simulate the fission damage and induce chemical mixing that occur within nuclear fuels. The dissolution experiment was conducted under a nitrogen atmosphere (200–900 O_2 ppm in N_2) to study the effect of the induced irradiation damage and mixing on the dissolution of the UO_2 matrix. The irradiated samples showed a decrease in the amount of dissolved uranium, as compared to the corresponding unirradiated samples. This was ascribed to the irradiation-induced chemical mixing of the UO_2 films with the substrate elements, which resulted in stabilisation of the UO_2 matrix and increased its aqueous durability. Secondary phases were also observed on the surface of the UO_2 films after the dissolution experiment.

1. Introduction

Some countries have decided or are in a position to decide in favour of complete or partial geological disposal of spent nuclear fuel (SNF) [1]. A safety case assessment of any geological repository for SNF requires the prediction of the release rates of radioactive elements from the fuel once the containers fail and contact with groundwater is established [2,3]. Despite a lot of effort being put into studying the different parameters relevant to the dissolution of spent nuclear fuel under geological disposal conditions [1–32] there are still some aspects that require further clarification.

For example, to the best of our knowledge there is only one publication in the open literature, produced by Matzke [25], which considers the effect of radiation damage on the dissolution of uranium dioxide matrix in water. About 80% (~170 MeV) of the energy liberated in a nuclear fission event is given to fission fragments as their kinetic energy and is transformed into heat by the interaction of the fast moving fragments with the crystal electrons and the crystal atoms in the fuel matrix [33]. This results in the fission damage which is manifested in a lattice parameter increase and lattice strain, surface fission tracks, the high burn-up structure, enhanced diffusion, creep and so on, leading to the degradation of the fuel's properties [34–37].

Another important aspect which received a limited attention is the dissolution of the high burn-up structure [5,30–32]. The high burn-up structure is a scientifically interesting and technologically important phenomenon [38]. Fuel pellets with an average burn-up above ~45 GWd/tU [37] show a crystallographic restructuring at the peripheral region, called the 'rim structure' or 'high burn-up structure' [39]. This structure is characterised by the existence of highly dense small sub-grains with a size of around 100 nm and the accumulation of small pores with an average size of about 1 μm [39]. This restructuring can influence the fuel performance by affecting fission gas release, fuel temperature, hardness, swelling and so forth [39]. The high concentration of fission products and Pu together with the small grain size near the surface of the fuel pellet are of concern for spent nuclear fuel storage and geological disposal since in the case of water access, leaching starts in this region,

* Corresponding author.
E-mail address: apopel@cantab.net (A.J. Popel).

http://dx.doi.org/10.1016/j.jallcom.2017.05.084

which has the highest radiotoxicity [38]. Thus, the high burn-up structure has been studied widely [36,39–53]. However, the exact mechanism, the kinetics and the extent of its formation are still unclear [37,41,43,47].

Dissolution rate and solubility of uranium dioxide in aqueous environment are strongly dependant on uranium oxidation state, as U^{6+} is more soluble than U^{4+} by several orders of magnitude [14]. As a result, oxidation of UO_2 increases its solubility by almost five orders of magnitude [11]. Another key factor which determines the kinetics of uranium dioxide dissolution is its solid-state conductivity [2,3]. Nakae et al. [54] showed that the dependence of electrical conductivity of UO_2 on radiation damage is rather complex, but generally the radiation damage results in a decrease of the electrical conductivity of UO_2.

Although the original intent of our work was to assess the explicit effect of radiation damage by fission-energy ions on the dissolution of the UO_2 matrix to contribute to the gap knowledge in this field, we induced some chemical mixing between the UO_2 film and the substrate elements (La, Sr, Al, Ta, O). However, we do believe that the produced complex chemical system with the accumulated radiation damage is relevant for understanding the dissolution of the high burn-up structure [5]. Hence, the current work considers the effect of radiation damage and the associated chemical mixing between the UO_2 film and the substrate elements on aqueous durability of the modified UO_2 matrix.

For this purpose, thin films of UO_2 dioxide on LSAT (Lanthanum Strontium Aluminium Tantalum oxide) substrates were produced and irradiated by 92 MeV $^{129}Xe^{23+}$ ions to a fluence of 4.8×10^{15} ions/cm^2 to simulate the fission damage that occurs within nuclear fuels [55]. The results of thorough characterisation of the irradiated and as-produced thin films were published in Refs. [55,56]. A 95-day static batch dissolution experiment was conducted under a nitrogen atmosphere. The uranium concentration in the sampled solutions was determined by ICP-MS (Inductively Coupled Plasma Mass Spectrometry). After the dissolution experiment the surfaces of the samples were characterised using SEM (Scanning Electron Microscopy), EDX (Energy Dispersive X-ray spectroscopy), AFM (Atomic Force Microscopy) and XRD (X-ray Diffraction) techniques.

2. Experimental details

2.1. Sample production and irradiation

Thin films of uranium dioxide were produced by reactive sputtering onto single crystal LSAT substrates with (001), (110) and (111) crystallographic orientations as described in detail in Ref. [55]. Table 1 summarises the samples produced. Post fabrication, the thin films (and substrates) were cut into two halves using a diamond saw, such that one half could be used for ion irradiation, whilst the other half was left as a control for comparison measurements. The irradiated halves are denoted by an asterisk,*, in the sample numbering scheme.

Table 1
Summary of the crystallographic indices (*hkl*) for the substrates and UO_2 films and thicknesses of the UO_2 films measured using transverse SEM on a cross section of each sample [55].

Sample name	(*hkl*)		Film thickness (nm) (±10%)
	LSAT substrate	UO_2 film	
SN489	(111)	(210)[a]	110
SN490	(001)	(001)	140
SN491	(001)	(001)	120
SN492	(110)	(111)[a]	140

[a] Preferential crystallographic orientation.

To simulate the damage produced by fission fragments in nuclear fuel, the samples were irradiated with 92 MeV energy $^{129}Xe^{23+}$ ions to a fluence of 4.8×10^{15} ions/cm^2 on the IRRSUD beamline at the GANIL accelerator, Caen, France with a detailed description given in Ref. [55]. The SRIM code [57] indicated that the Xe ions completely penetrate the UO_2 thin films (140 nm max) and the electronic stopping regime dominates the dissipation of ion energy throughout the entire film. The Xe ions stop in the substrate at a depth of ~7.3 μm beneath the sample's surface [55].

2.2. Dissolution experiment

The 5 × 10 mm halves of the irradiated and as-produced samples were cut further into 5 × 5 mm sections. One set of the produced 5 mm squares of the original samples was used for dissolution experiments, whereas the other set was retained for further measurements.

The dissolution experiment was conducted in a glove box under nitrogen atmosphere with the level of oxygen in the range 200–900 ppm. Deionised Milli-Q water (18.2 MΩ/cm) was bubbled with nitrogen over night before it was introduced into the glove box to reduce the amount of dissolved oxygen. The samples were prewashed by placing them into vials containing 3 ml of the deionised water for 5 h. Then, the samples were rinsed with the deionised water, gently dried with a tissue and placed into dissolution vessels containing 5 ml of the deionised water. Static replenishment tests were run where ~1 ml of the solution sample was taken out into a vial at various intervals and ~1 ml of the deionised water was replenished. All vessels were tightly closed to prevent water evaporation. Two leaching vessels were filled with 5 ml of deionised and deoxygenated water as control blanks. The amount of the solution transferred from the dissolution vessels into the vials was monitored by weighting empty and filled vials. The dissolution experiment was performed at an ambient temperature of ~20 °C for 95 days.

Each aliquot of solution was acidified with 0.15 μm of 15.5 M HNO_3 and analysed on a Perkin Elmer SCIEX Elan DRC II quadrupole ICP-MS. The concentrations presented in Section 3.2 were corrected for the acid additions and represent U concentration before the dilution. The calibration standards for U, La, Sr, Al and Ta were prepared as an external calibration using serial dilutions of standards (blank, 0.01, 0.05, 0.1, 1, 10, 100 ppb (mass basis)) prepared from single element high purity standards (CPI, California, USA) in high purity 1 vol% HNO_3 (quartz distilled in house). The ICP-MS internal standards were 10 ppb Rh and In in 1 vol% HNO_3, added online with a t-piece and mixing tube prior to the nebuliser. An independently prepared quality control standard, containing uranium among other elements at 0.25 ppb (mass basis), (SPS-SW2, LGC Standards, UK) was repeatedly analysed throughout the run to check for calibration accuracy (approx. 5%) with a similar precision. Instrumental drift was less than 5% measured for the raw intensity of the internal standards during the entire analytical run. ICP-MS sensitivity in this configuration was 5×10^4 cps/ppb In with CeO/Ce ratios = 3%. Concentrations results were calculated by the Elan v3.4 software with a simple linear calibration line and intercept set to zero. The raw intensities were blank subtracted and internal standard normalised before calibration calculations were performed.

2.3. Post-dissolution sample characterisation

Following the dissolution experiment, the irradiated and as-produced samples were analysed using SEM, EDX, AFM and XRD techniques in attempt to detect and characterise any secondary phase formations. SEM images were obtained using a Zeiss Leo

Supra 50VP scanning electron microscope equipped with an X-Max 80 mm^2 EDX detector (Oxford Instruments). To reduce the charging effects on the sample, the analysis was performed in a low-vacuum regime, with a 39 Pa pressure of nitrogen and a variable pressure secondary electron (VPSE) detector used to acquire images. Surface composition was examined using EDX. The EDX spectral deconvolution and elemental quantification were performed using the INCA software (Oxford Instruments) with ZAF-correction. Before every series of EDX measurements, signal intensity was recalibrated in low-vacuum mode using a Co standard sample. AFM images were obtained on NT-MDT N'Tegra Aura atomic force microscope with the use of diamond ART-300 tips (Artech Carbon) with a radius of <10 nm and cantilever resonance frequency of approximately 300 kHz using the same setting as described in Ref. [55]. The samples were analysed in Bragg-Brentano geometry on a Rigaku D/MAX 2500 diffractometer with rotating copper anode and curved graphite [002] monochromator for Cu Kα1,2 installed on the secondary beam. Samples were spun during signal collection in all cases.

3. Results

3.1. Sample characterisation

The unirradiated samples all were flat and AFM measurements (Fig. 1a) gave the root mean square roughness (RMS) as low as 0.35 nm and average height variation of 5.8 nm. The ion irradiation caused significant restructuring of the films (Fig. 1b): a discrete small grains (~3 μm), larger circular (up to ~40 μm) and linear formations were observed in AFM and SEM studies. XRD analysis showed that the ion irradiation caused some significant crystallographic rearrangements manifested by disappearance of some originally present and appearance of new UO_2 XRD reflections [55]. XPS analysis [56] showed (Table 2) that the as-produced films had the oxygen coefficient, k_O, values in the range 2.07–2.11 and the ion irradiation resulted in an increase of the k_O values up to 2.11–2.31 with the corresponding decrease in the relative proportion of U^{4+} and increase in the relative proportion of U^{5+} and U^{6+} ions at the surface of the UO_2 thin films.

EDX [55] and XPS [56] analyses indicated that significant substrate-film mixing took place as a result of the ion irradiation and the microstructure of the irradiated samples is not uniform in elemental composition. The readers are referred to Refs. [55] and [56] for more details on characterisation of the as-produced and irradiated samples.

3.2. Dissolution results

pH and Eh values of the solutions were measured at the end of the dissolution experiment once the samples were removed from the solutions. pH values were in the range 6.4–6.6 and Eh values in the bulk of solutions were in the range +200–240 mV measured by a combined electrode consisting of a Pt working electrode relative to the Ag|AgCl reference electrode in 3 M KCl solution (or +407–447 mV relative to the standard hydrogen electrode), and were similar to the values of the deionised water.

The regular analysis of the 0.25 ppb U quality control standard showed a maximum error in U concentration of 9%. The measured U concentration for the blank runs was in the range $0–1 \times 10^{-11}$ mol/l. Hence, the measurement error of 9% or $\pm 1 \times 10^{-11}$ mol/l, whichever is greater, should be applied to the obtained U concentration values. The error bars are not plotted on the dissolution graphs (Figs. 2 and 3) for the sake of clarity as their sizes do not affect the observed trends.

Fig. 2 shows a plot of U concentration as a function of dissolution time for the irradiated and as-produced samples and Fig. 3 presents the dissolution curves for the irradiated samples separately for clarity.

Table 2
Summary of the XPS results: the oxygen coefficient k_O at the surface of the UO_2 thin films with the corresponding composition of uranium ions k(%) [56].

Sample	k_O in UO_{2+x} (±0.01)	k (%)		
		U^{4+}	U^{5+}	U^{6+}
SN489	2.11	44	45	11
SN489*	2.31	0.3	68	31
SN490	2.07	58	35	7
SN490*	2.11	44	45	11
SN491	2.08	52	39	9
SN491*	2.14	33	52	14
SN492	2.10	48	42	10
SN492*	2.17	25	57	17

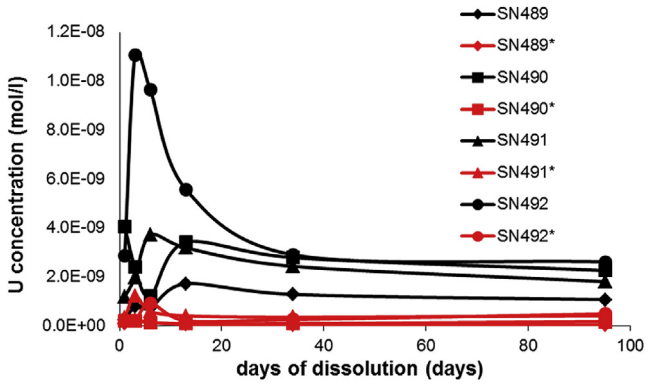

Fig. 2. A plot of U concentration as a function of dissolution time for the thin film samples of UO_2 on LSAT substrates. The solid lines are only added to guide the eye.

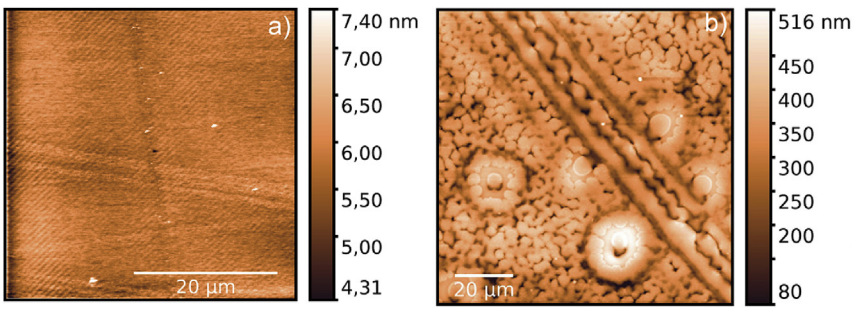

Fig. 1. AFM images of the surface topography [55]: a) unirradiated sample SN492, the regular fluctuations are attributed to instrumental effects for a very flat surface; b) the corresponding irradiated sample SN492*.

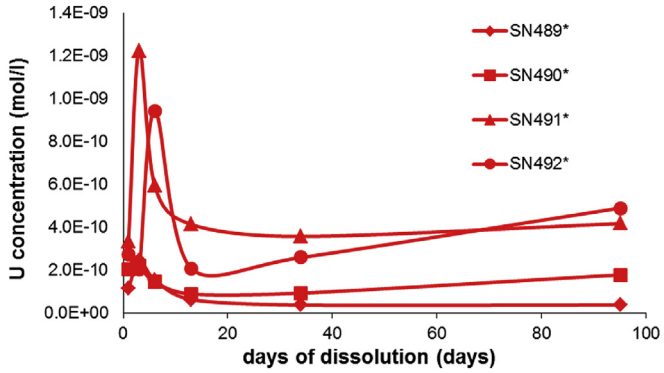

Fig. 3. A plot of U concentration as a function of leaching time for the irradiated thin film samples of UO_2 on LSAT substrates. The solid lines are only added to guide the eye.

The uranium concentration ratios for SN489/SN489*, SN490/SN490*, SN491/SN491* and SN492/SN492* sample pairs were 28, 13, 4.3 and 5.3, respectively, on the 95-th day of dissolution. Uranium concentration values at the end of the experiment were in the range 1.1×10^{-9}–2.6×10^{-9} mol/l for the unirradiated samples and in the range 4×10^{-11}–4.9×10^{-9} mol/l for the irradiated samples. Both the transient release and the final concentration of uranium from the unirradiated samples were higher than for the unirradiated samples.

The XPS study [56] showed that sample SN490 had a higher carbonaceous contamination of the surface than other unirradiated samples. This carbonaceous layer could act as a barrier for water contact with the UO_{2+x} surface. As a result, sample SN490 showed lower U concentration in the pre-wash solution and a delayed release of uranium, as compared to sample SN491. For irradiated samples SN490* and SN491* the relative separation between the dissolution curves is higher than for unirradiated pair SN490/SN491, which correlates well with a higher difference in the oxygen coefficient and uranium ionic composition – see Table 2. Sample SN489*, which almost had no U^{4+} ions (Table 2), showed the highest uranium concentration (3×10^{-8} mol/l) in the pre-wash solution as compared to samples SN490*–SN492* (2×10^{-11}–2.1×10^{-10} mol/l). This observation is consistent with the fact that uranium in higher oxidation states is more soluble than in the oxidation state 4+ [11]. For other samples there is no apparent correlation between the surface composition and the measured uranium concentration values.

The presence of maximum in the dissolution curves indicates that precipitation of uranium containing secondary phases is likely to take place – dissolution-precipitation behaviour is expected. On the last day of dissolution the dissolution curves for all unirradiated samples showed negative gradient indicating that further decline in U concentration is likely to happen with time due to continuing formation of secondary phases.

Among the unirradiated samples, sample SN492 showed the highest measured U concentration values at the beginning of dissolution and then the values converged towards the measured values for samples SN490 and SN491. Sample SN489 showed the lowest U measured values and samples SN490 and SN491 showed intermediate measured U concentration values. From this observation it is possible to make a conclusion that samples with the expected single domain of UO_2 crystal growth ((210) for SN489 and (001) for SN490 and SN491) have higher resistance to dissolution than samples with multiple domains of UO_2 crystal growth ((111), (110) and (311) for SN492).

On the last day of dissolution the dissolution curves for all irradiated samples, except for sample SN489* (zero gradient), have positive gradients indicating that increase in U concentration is likely to happen with time. This observation is consistent with the work by Serrano-Purroy et al. [31], where it was observed that it took longer for the samples from the outer part of the irradiated fuel pellet (higher burn-up) to reach the same solubility value than for the samples from the inner part of the fuel pellet (lower burn-up). The reason for this behaviour is not clear. It can be the case that surface restructuring (oxidation in the work by Serrano-Purroy et al. [31] and, possibly, surface amorphisation [13] during the dissolution in our work) results in a destabilising effect of the dopants against oxidative dissolution of the UO_2 matrix (discussed in Section 4).

Among the irradiated samples, sample SN489* showed the dissolution curve with the lowest measured U concentration values followed by sample SN490*. The dissolution curve for sample SN491* showed mainly the highest U concentration values, but the dissolution curve for sample SN492* exceeded them towards the end of dissolution. From the observed trend in the measured uranium concentration values of the irradiated samples it is impossible to comment on the effect of the initial crystal growth domains on post-irradiation dissolution.

3.3. Post-dissolution results

EDX analysis showed that uranium remained on the surface of the unirradiated and irradiated samples. Hence, there was no complete uranium oxide dissolution from the samples. SEM (Fig. 4) and AFM (Fig. 5) analyses revealed that a secondary phase in the form of tubes with a length in the range of 5–10 μm and a diameter of ~0.5 μm was formed at the surface of the unirradiated samples during the dissolution experiment.

In addition, AFM and SEM (not shown) analyses also indicated that a secondary phase in the form of circular grains with a diameter in the range of 0.15–0.5 μm was formed (Fig. 6). It is not clear if the composition of the grain shape secondary phase is identical to the tube shape secondary phase.

Secondary phases were not observed on the surface of the irradiated samples, however this may be due to the higher surface roughness of the samples, which makes discrimination of surface precipitates more difficult. The high surface roughness of the irradiated samples suggests that it will be difficult to achieve a continuous coverage of the surface by secondary phases. This can explain why an increase in uranium concentration is observed

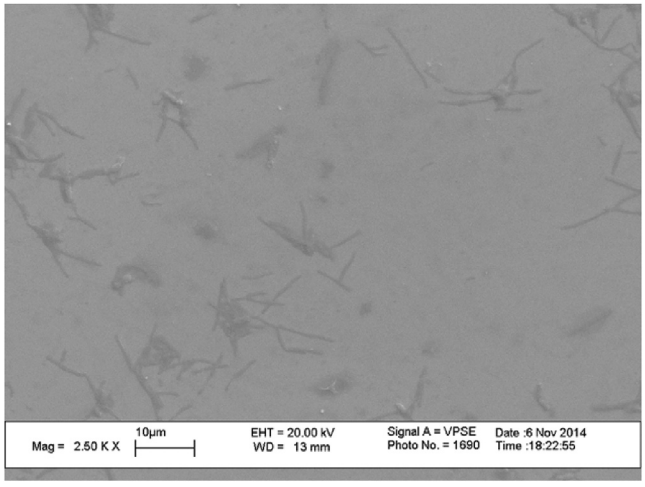

Fig. 4. A secondary electron SEM image of the surface topography of sample SN489 after the dissolution showing a tube-shape secondary phase.

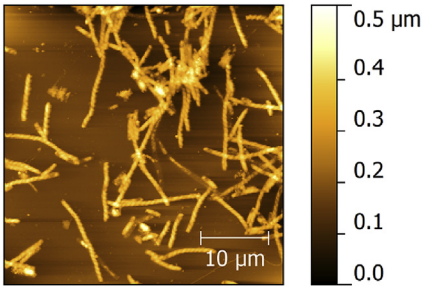

Fig. 5. An AFM image of the surface topography of sample SN491 after the dissolution showing a tube-shape secondary phase.

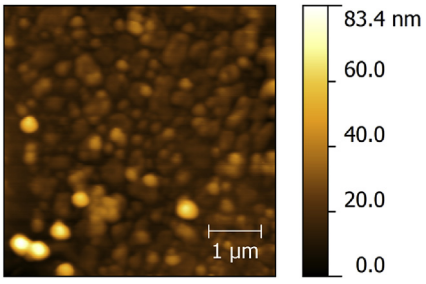

Fig. 6. An AFM image of the surface topography of sample SN490 after the dissolution showing a grain-shape secondary phase.

towards the end of the dissolution experiment – dissolution of uranium from regions not coated with surface precipitates might be taking place.

XRD analysis in standard Bragg-Brentano geometry did not reveal any signal from secondary phases, most likely due to the low amount or amorphous nature of the secondary phases present at the surface of the samples.

4. Discussion

A lower uranium concentration was measured from aliquots taken from a solution in contact with the irradiated UO_2 thin film samples compared with the unirradiated samples. The measured Eh values (+166–206 mV vs SCE) indicate that the UO_2 films should have been subjected to oxidative dissolution [2,3]. The observed trend can be rationalised in the same way as in the work of by Serrano-Purroy et al. [31] on real spent nuclear fuel, where the reduced dissolution rate of the samples from the outer region of the irradiated fuel pellets (higher burn-up: more radiation damage and fission products) were compared with the samples taken from the inner region of the fuel pellets (lower burn-up: less radiation damage and fission products). The implication was that the greater incorporation of fission products in the high burn-up region inhibited the dissolution of the UO_2 matrix. The ion irradiation caused chemical mixing [58,59] of the UO_2 film with the substrate elements (La, Sr, Al, Ta), as was observed in the EDX [55] and XPS [56] analyses of the irradiated samples. The substrate elements are expected to have a stabilising effect on the UO_2 lattice and increase its oxidative dissolution resistance. The most promising substrate element is La, as it is a trivalent rare earth element with the best size match with U^{4+} ions ($r_{cr}(La^{3+}) > r_{cr}(U^{4+})$ by 14% [60]). There are several possible explanations for this enhancement of the dissolution UO_2 resistance by lanthanide incorporation. McEachern and Taylor [61] suggested that larger substitutional ions can provide stabilisation of the UO_2 matrix from oxidation by limiting the number of oxygens that can fit into interstitials in the fluorite-type structure. Razdan and Shoesmith [8] considered formation of dopant-oxygen vacancy clusters that result in a reduction in availability of the interstitial sites required for the incorporation of interstitial oxygen during the oxidation. Park and Olander [62] showed that trivalent rare earth dopants act as effectively negative charge and repel neighbouring interstitial oxygen ions, causing elimination of interstitial sites for oxygen occupation. As a result, Casella et al. [27] and Razdan and Shoesmith [8] observed that doping of UO_2 matrix with rare earth elements caused a significant decrease in the oxidative dissolution rate. In addition, the high fluence irradiation could result in a reduced electrical conductivity of the UO_2 matrix [54], which leads to a reduced dissolution rate [2,3]. Hence, our observation is consistent with some of the previous studies [8,27,31]. However, our observation is not consistent with the work by Matzke [25], where an increase in the dissolution rate was observed after irradiating UO_2 and UO_2-based simfuel with 40 and 45 keV ions, and with the work on CeO_2 samples (inactive analogue to UO_2) [63] irradiated by the same 92 MeV Xe ions. The main reason for this discrepancy is attributed to be the ion-beam-induced chemical mixing of the UO_2 film with the substrate elements which took place in this work.

The measured uranium concentration values at the end of the dissolution experiment were in the range 4×10^{-11}–2.6×10^{-9} mol/l. This implies that only secondary phases with the solubility values lower than these could precipitate out of solution. In terms of uranium based secondary phases, only coffinite ($USiO_4$) and crystalline UO_2 [28] meet the criterion. However, coffinite formation requires elevated temperature (180 °C) and high excess of Si(aq) (~10^{-2} mol/l) [19]. Hence, coffinite formation is unlikely. As was noted by Neck and Kim [13], tetravalent actinide ions have a strong tendency towards colloid formation. Hence, formation of colloidal UO_2 cannot be excluded, but the formed colloids have to be crystalline to meet the solubility requirement for precipitation. Batuk [29] performed dissolution of uranium dioxide samples in solution simulating a groundwater under air atmosphere at temperatures of 70 and 150 °C and observed formation of nano-size crystalline UO_2 particles on the surface of the samples and in the solution. It was suggested that these colloidal crystalline UO_2 particles covered the surface of the uranium dioxide samples and inhibited further oxidation. Unfortunately, no explanation was given as to why these colloidal UO_2 particles did not oxidise. In addition, low solubility deposits containing Ca and Si could form on the surface of the films and inhibited further dissolution [3]. Calcium was detected in the sampled solutions by the ICP-MS analysis at a concentration of ~100 ppb and more likely was taken up from the experimental set-up environment as a contaminant. Silicon is also expected to be present as a contaminant at a similar concentration.

The secondary phases observed in Figs. 5 and 6 are more likely formed by substrate elements and other elements taken up in low concentrations from the experimental set-up environment (Pb, Na, Mg, Ca, Zn, Si, etc.), as they were present in solutions in excessive concentrations over uranium. Inclusion of U into these phases is likely to happen, as uranium is often found as a component of minor concentration in many mineral phases [19]. Further work is required to identify these phases.

In this experiment the onset of the secondary phase formation limits the maximum uranium concentration attained in the solution. In addition, precipitation of secondary phases, for example, of crystalline colloidal UO_2 and/or Ca-Si low solubility deposits, can block the UO_2 surface from further dissolution. Hence, in the experiments reported in this paper, the rate of the UO_2 surface coverage by less soluble secondary phases can be considered as the overall dissolution rate-controlling step. However, in the case of a real geological repository, the near field around the spent fuel may

experience more oxidising conditions due to alpha-radiolysis than the far field. Hence, precipitation of secondary phases may shift from taking place mainly on the fuel to the far field with more reducing conditions [22]. Hence, under this real scenario the effect of the secondary phases on the overall dissolution process may be reduced.

5. Conclusions

This work focused on the relative dissolution behaviour of irradiated and unirradiated UO_2 thin film samples under specific controlled conditions. The unirradiated samples showed consistently higher measured U concentration values than the corresponding irradiated samples. This observation is consistent with the case of real spent nuclear fuel dissolution, when it is was observed that the fuel samples taken from the outer part of the irradiated pellet (higher burn-up) showed lower dissolution rate than the fuel samples taken from the central part of the pellet (lower burnup) [31], and with the work by Casella et al. [27] and Razdan and Shoesmith [8] on the oxidative dissolution of doped UO_2. It was suggested that the irradiation-induced chemical mixing with the substrate elements, observed by the EDX and XPS analyses [55,56], had a stabilising effect on the UO_2 matrix and increased UO_2 dissolution resistance.

Samples with expected single domain of UO_2 crystal growth showed lower measured U concentration values than samples with multiple domains of UO_2 crystal growth. From the observed trend in the measured uranium concentration values for the irradiated samples it was not possible to comment on the effect of the initial crystal growth domain on post-irradiation dissolution.

Tube and grain shape secondary phases were observed on the surface of the unirradiated samples and further work is required for their characterisation.

Supporting data

Supporting data will be available in A.J. Popel's PhD thesis (University of Cambridge) published online.

Acknowledgments

The irradiation experiment was performed at the Grand Accélérateur National d'Ions Lourds (GANIL) Caen, France, and supported by the French Network EMIR. The support in planning and execution of the experiment by the CIMAP-CIRIL staff and the GANIL technical staff, especially, I. Monnet, C. Grygiel, T. Madi and F. Durantel, is much appreciated. Thanks also go to O.N. Batuk for fruitful discussions on UO_2 dissolution. AFM, SEM and EDX experiments were performed with support of M.V.Lomonosov Moscow State University Program of Development. A.J. Popel acknowledges funding from the UK EPSRC (grant EP/I036400/1) and Radioactive Waste Management Ltd (formerly the Radioactive Waste Management Directorate of the UK Nuclear Decommissioning Authority, contract NPO004411A-EPS02), a maintenance grant from the Russian Foundation for Basic Research (projects 13-03-90916) and CSAR bursary.

References

[1] D. Cui, E. Ekeroth, P. Fors, K. Spahiu, The interaction of dissolved hydrogen with spent fuel or UO_2 doped with alpha emitters, Mater. Res. Soc. Symp. Proc. 1104 (2008).
[2] D.W. Shoesmith, S. Sunder, The prediction of nuclear fuel (UO_2) dissolution rates under waste disposal conditions, J. Nucl. Mater. 190 (1992) 20–35.
[3] D.W. Shoesmith, Fuel corrosion processes under waste disposal conditions, J. Nucl. Mater. 282 (2000) 1–31.
[4] R. Springell, S. Rennie, L. Costelle, J. Darnbrough, C. Stitt, E. Cocklin, C. Lucas, R. Burrows, H. Sims, D. Wermeille, J. Rawle, C. Nicklin, W. Nuttall, T. Scott, G. Lander, Water corrosion of spent nuclear fuel: radiolysis driven dissolution at the UO_2/water interface, Faraday Discuss. 180 (2015) 301–311.
[5] T. Fanghänel, V.V. Rondinella, J.P. Glatz, T. Wiss, D.H. Wegen, T. Gouder, P. Carbol, D. Serrano-Purroy, D. Papaioannou, Reducing uncertainties affecting the assessment of the long-term corrosion behavior of spent nuclear fuel, Inorg. Chem. 52 (2013) 3491–3509.
[6] M. Razdan, D.W. Shoesmith, The influence of hydrogen peroxide and hydrogen on the corrosion of simulated spent nuclear fuel, Faraday Discuss. 180 (2015) 283–299.
[7] M. Razdan, M. Trummer, D. Zagidulin, M. Jonsson, D.W. Shoesmith, Electrochemical and surface characterization of uranium dioxide containing rare-earth oxide (Y_2O_3) and metal (Pd) particles, Electrochim. Acta 130 (2014) 29–39.
[8] M. Razdan, D.W. Shoesmith, Influence of trivalent-dopants on the structural and electrochemical properties of uranium dioxide (UO_2), J. Electrochem. Soc. 161 (2014) H105–H113.
[9] L. Wu, Y. Beauregard, Z. Qin, S. Rohani, D.W. Shoesmith, A model for the influence of steel corrosion products on nuclear fuel corrosion under permanent disposal conditions, Corros. Sci. 61 (2012) 83–91.
[10] H. He, Z. Qin, D.W. Shoesmith, Characterizing the relationship between hyperstoichiometry, defect structure and local corrosion kinetics of uranium dioxide, Electrochim. Acta 56 (2010) 53–60.
[11] H. He, R.K. Zhu, Z. Qin, P. Keech, Z. Ding, D.W. Shoesmith, Determination of local corrosion kinetics on hyper-stoichiometric UO_{2+x} by scanning electrochemical microscopy, J. Electrochem. Soc. 156 (2009) C87–C94.
[12] D.W. Shoesmith, S. Sunder, M.G. Bailey, G.J. Wallace, The corrosion of nuclear fuel (UO_2) in oxygenated solutions, Corros. Sci. 29 (1989) 1115–1128.
[13] V. Neck, J.I. Kim, Solubility and hydrolysis of tetravalent actinides, Radiochim. Acta 89 (2001) 1–16.
[14] K. Opel, S. Weiß, S. Hübener, H. Zänker, G. Bernhard, Study of the solubility of amorphous and crystalline uranium dioxide by combined spectroscopic methods, Radiochim. Acta 95 (2007) 143–149.
[15] S. Sundin, B. Dahlgren, O. Roth, M. Jonsson, H_2O_2 and radiation induced dissolution of UO_2 and SIMFUEL in deficient aqueous solution, J. Nucl. Mater. 443 (2013) 291–297.
[16] D.E. Giammar, J.M. Cerrato, V. Mehta, Z. Wang, Y. Wang, T.J. Pepping, K.U. Ulrich, J.S. Lezama-Pacheco, J.R. Bargar, Effect of diffusive transport limitations on UO_2 dissolution, Water Res. 46 (2012) 6023–6032.
[17] O.N. Batuk, S.N. Kalmykov, E.V. Zakharova, Y.A. Teterin, B.F. Myasoedov, Uranium dioxide interaction with groundwater – leaching behavior and sorption tests, J. Nucl. Mater. 352 (2006) 241–245.
[18] E.M. Pierce, J.P. Icenhower, R.J. Serne, J.G. Catalano, Experimental determination of UO_2(cr) dissolution kinetics: effects of solution saturation state and pH, J. Nucl. Mater. 345 (2005) 206–218.
[19] M. Amme, T. Wiss, H. Thiele, P. Boulet, H. Lang, Uranium secondary phase formation during anoxic hydrothermal leaching processes of UO_2 nuclear fuel, J. Nucl. Mater. 341 (2005) 209–223.
[20] T. Mennecart, B. Grambow, M. Fattahi, Z. Andriambololona, Effect of alpha radiolysis on doped UO_2 dissolution under reducing conditions, Radiochim. Acta 92 (2004) 611–615.
[21] K.-U. Ulrich, E.S. Ilton, H. Veeramani, J.O. Sharp, R. Bernier-Latmani, E.J. Schofield, J.R. Bargar, D.E. Giammar, Comparative dissolution kinetics of biogenic and chemogenic uraninite under oxidizing conditions in the presence of carbonate, Geochim. Cosmochim. Acta 73 (2009) 6065–6083.
[22] G. Rousseau, M. Fattahi, B. Grambow, F. Boucher, G. Ouvrard, Coprecipitation of thorium with UO_2, Radiochim. Acta 90 (2002) 523–527.
[23] V.V. Rondinella, J. Cobos, Hj. Matzke, T. Wiss, P. Carbol, D. Solatie, Leaching behavior and α-Decay damage accumulation of UO_2 containing short-lived actinides, Mater. Res. Soc. Symp. Proc. 663 (2001).
[24] V.V. Rondinella, Hj. Matzke, J. Cobos, T. Wiss, α-radiolysis and α-radiation damage effects on UO_2 dissolution under spent fuel storage conditions, Mater. Res. Soc. Symp. Proc. 556 (1999).
[25] Hj. Matzke, Radiation damage-enhanced dissolution of UO_2 in water, J. Nucl. Mater. 190 (1992) 101–106.
[26] J. Bruno, I. Casas, I. Puigdomènech, The kinetics of dissolution of UO_2 under reducing conditions and the influence of an oxidized surface layer (UO_{2+x}): application of a continuous flow-through reactor, Geochim. Cosmochim. Acta 55 (1991) 647–658.
[27] A. Casella, B. Hanson, W. Miller, The effect of fuel chemistry on UO_2 dissolution, J. Nucl. Mater. 476 (2016) 45–55.
[28] S. Guilbert, M.J. Guittet, N. Barré, P. Trocellier, M. Gautier-Soyer, Z. Andriambololona, Dissolution of uranium dioxide in simulated Boom clay water, Radiochim. Acta 90 (2002) 75–80.
[29] O.N. Batuk, Behaviour of Uranium Dioxide under Oxidative Hydrothermal Conditions, PhD thesis, Lomonosov Moscow State University, 2007 (in Russian).
[30] K. Lemmens, E. González-Robles, B. Kienzler, E. Curti, D. Serrano-Purroy, R. Sureda, A. Martínez-Torrents, O. Roth, E. Slonszki, T. Mennecart, I. Günther-Leopold, Z. Hózer, Instant release of fission products in leaching experiments with high burn-up nuclear fuels in the framework of the Euratom project FIRST-Nuclides, J. Nucl. Mater. 484 (2017) 307–323.
[31] D. Serrano-Purroy, F. Clarens, E. González-Robles, J.P. Glatz, D.H. Wegen, J. de Pablo, I. Casas, J. Giménez, A. Martínez-Esparza, Instant release fraction and

matrix release of high burn-up UO_2 spent nuclear fuel: effect of high burn-up structure and leaching solution composition, J. Nucl. Mater. 427 (2012) 249–258.
[32] P. Fors, P. Carbol, S. Van Winckel, K. Spahiu, Corrosion of high burn-up structured UO_2 fuel in presence of dissolved H_2, J. Nucl. Mater. 394 (2009) 1–8.
[33] H. Blank, Properties of fission spikes in UO_2 and UC due to electronic stopping power, Phys. Status Solidi A 10 (1972) 465–478.
[34] P.B. Weisensee, J.P. Feser, D.G. Cahill, Effect of ion irradiation on the thermal conductivity of UO_2 and U_3O_8 epitaxial layers, J. Nucl. Mater. 443 (2013) 212–217.
[35] N. Ishikawa, Y. Chimi, O. Michikami, Y. Ohta, K. Ohhara, M. Lang, R. Neumann, Study of structural change in CeO_2 irradiated with high-energy ions by means of X-ray diffraction measurement, Nucl. Instrum. Metheds Phys. Res. B 266 (2008) 3033–3036.
[36] Hj. Matzke, P.G. Lucuta, T. Wiss, Swift heavy ion and fission damage effects in UO_2, Nucl. Instrum. Metheds Phys. Res. B 166–167 (2000) 920–926.
[37] Hj. Matzke, Radiation damage in nuclear materials, Nucl. Instrum. Metheds Phys. Res. B 65 (1992) 30–39.
[38] Hj. Matzke, A. Turos, G. Linker, Polygonization of single crystals of the fluorite-type oxide UO_2 due to high dose ion implantation, Nucl. Instrum. Metheds Phys. Res. B 91 (1994) 294–300.
[39] T. Sonoda, M. Kinoshita, N. Ishikawa, M. Sataka, A. Iwase, K. Yasunaga, Clarification of high density electronic excitation effects on the microstructural evolution in UO_2, Nucl. Instrum. Metheds Phys. Res. B 268 (2010) 3277–3281.
[40] V.G. Baranov, A.V. Lunev, A.V. Tenishev, A.V. Khlunov, Interaction of dislocations in UO_2 during high burn-up structure formation, J. Nucl. Mater. 444 (2014) 129–137.
[41] V.G. Baranov, A.V. Lunev, V.F. Reutov, A.V. Tenishev, M.G. Isaenkova, A.V. Khlunov, An attempt to reproduce high burn-up structure by ion irradiation of SIMFUEL, J. Nucl. Mater. 452 (2014) 147–157.
[42] N. Nakae, H. Akiyama, H. Miura, T. Baba, K. Kamimura, S. Kurematsu, Y. Kosaka, A. Yoshino, T. Kitagawa, Thermal property change of MOX and UO_2 irradiated up to high burnup of 74GWd/t, J. Nucl. Mater. 440 (2013) 515–523.
[43] V.V. Rondinella, T. Wiss, The high burn-up structure in nuclear fuel, Mater. Today 13 (2010) 24–32.
[44] M. Kinoshita, K. Yasunaga, T. Sonoda, A. Iwase, N. Ishikawa, M. Sataka, K. Yasuda, S. Matsumura, H.Y. Geng, T. Ichinomiya, Y. Chen, Y. Kaneta, M. Iwasawa, T. Ohnuma, Y. Nishiura, J. Nakamura, Hj. Matzke, Recovery and restructuring induced by fission energy ions in high burnup nuclear fuel, Nucl. Instrum. Metheds Phys. Res. B 267 (2009) 960–963.
[45] C.T. Walker, D. Staicu, M. Sheindlin, D. Papaioannou, W. Goll, F. Sontheimer, On the thermal conductivity of UO_2 nuclear fuel at a high burn-up of around 100MWd/kgHM, J. Nucl. Mater. 350 (2006) 19–39.
[46] T. Sonoda, M. Kinoshita, I.L.F. Ray, T. Wiss, H. Thiele, D. Pellottiero, V.V. Rondinella, Hj. Matzke, Transmission electron microscopy observation on irradiation-induced microstructural evolution in high burn-up UO_2 disk fuel, Nucl. Instrum. Metheds Phys. Res. B 191 (2002) 622–628.
[47] N. Lozano, L. Desgranges, D. Aymes, J.C. Niepce, High magnification SEM observations for two types of granularity in a high burnup PWR fuel rim, J. Nucl. Mater. 257 (1998) 78–87.
[48] J. Cobos, D. Papaioannou, J. Spino, M. Coquerelle, Phase characterisation of simulated high burn-up UO_2 fuel, J. Alloys Compd. 271–273 (1998) 610–615.
[49] I.L.F. Ray, Hj. Matzke, H.A. Thiele, M. Kinoshita, An electron microscopy study of the RIM structure of a UO_2 fuel with a high burnup of 7.9% FIMA, J. Nucl. Mater. 245 (1997) 115–123.
[50] Hj. Matzke, J. Spino, Formation of the rim structure in high burnup fuel, J. Nucl. Mater. 248 (1997) 170–179.
[51] Hj. Matzke, M. Kinoshita, Polygonization and high burnup structure in nuclear fuels, J. Nucl. Mater. 247 (1997) 108–115.
[52] Hj. Matzke, Oxygen potential in the rim region of high burnup UO_2 fuel, J. Nucl. Mater. 208 (1994) 18–26.
[53] Hj. Matzke, On the rim effect in high burnup UO_2 LWR fuels, J. Nucl. Mater. 189 (1992) 141–148.
[54] N. Nakae, T. Koike, T. Kirihara, Electrical conductivity and thermoelectric power in irradiated UO_{2+x}, J. Nucl. Mater. 73 (1978) 217–221.
[55] A.J. Popel, V.A. Lebedev, P.G. Martin, A.A. Shiryaev, G.I. Lampronti, R. Springell, S.N. Kalmykov, T.B. Scott, I. Monnet, C. Grygiel, I. Farnan, Structural effects in UO_2 thin films irradiated with fission-energy Xe ions, J. Nucl. Mater. 482 (2016) 210–217.
[56] Y.A. Teterin, A.J. Popel, K.I. Maslakov, A.Y. Teterin, K.E. Ivanov, S.N. Kalmykov, R. Springell, T.B. Scott, I. Farnan, XPS study of ion irradiated and unirradiated UO_2 thin films, Inorg. Chem. 55 (2016) 8059–8070.
[57] J.F. Ziegler, J.P. Biersack, M.D. Ziegler, The Stopping and Range of Ions in Matter, SRIM Co., Chester, Maryland, U.S.A, 2008.
[58] C.M. Parish, P.D. Edmondson, Y. Zhang, M.K. Miller, Direct observation of ion-irradiation-induced chemical mixing, J. Nucl. Mater. 418 (2011) 106–109.
[59] P.D. Edmondson, N.P. Young, C.M. Parish, S. Moll, F. Namavar, W.J. Weber, Y. Zhang, T. Mitchell, Ion-beam-induced chemical mixing at a nanocrystalline CeO_2-Si interface, J. Am. Ceram. Soc. 96 (2013) 1666–1672.
[60] R.D. Shannon, Revised effective ionic radii and systematic studies of interatomie Distances in halides and chaleogenides, Acta Cryst. A32 (1976) 751–767.
[61] R.J. McEachern, P. Taylor, A review of the oxidation of uranium dioxide at temperatures below 400 °C, J. Nucl. Mater. 254 (1998) 87–121.
[62] K. Park, D.R. Olander, Defect models for the oxygen potentials of gadolinium- and europium-doped urania, J. Nucl. Mater. 187 (1992) 89–96.
[63] A.J. Popel, S. Le Solliec, G.I. Lampronti, J. Day, P.K. Petrov, I. Farnan, The effect of fission-energy Xe ion irradiation on the structural integrity and dissolution of the CeO_2 matrix, J. Nucl. Mater. 484 (2017) 332–338.